Tellus (1984), *36A*, 147–156

Stochastic orographic forcing of barotropic β-plane flow

By JOSEPH EGGER, *Meteorologisches Institut der Universität München, Theresienstrasse 37, D-8000 München 2, F. R. Germany*

(Manuscript received November 12, 1982; in final form May 5, 1983)

ABSTRACT

The zonal flow of the atmosphere varies erratically in time, thus providing stochastic sources and sinks of vorticity at the slopes of mountains. The atmospheric response to this stochastic forcing is studied using the linear barotropic vorticity equation for β-plane channel flow. Given the power spectrum of the zonal flow according to observations, the power spectrum of the atmospheric response can be evaluated. First a sinusoidal mountain is prescribed where a rather complete understanding of the resulting power fields can be obtained. Then a circular mountain is exposed to the random variations of the zonal flow and the resulting patterns are found to be in agreement with what one would expect on the basis of the theory of Rossby wave packets in channels. Third the northern hemisphere response is studied and it is concluded that the interaction of the stochastically varying zonal flow with the orography does not strongly contribute to the atmospheric low-frequency variability.

1. Introduction

The monthly mean fields of the northern hemisphere flow show pronounced waves at middle latitudes. A large number of theoretical papers have appeared since the pioneering work by Charney and Eliassen (1949) in order to explain the amplitude and phase of these stationary waves. The approach to the problem was almost invariably the same: one tried to derive the steady-state atmospheric response (frequency $\omega = 0$) to time mean forcing as provided by the orography and the geographically fixed heat sources. Linear models based on these ideas reproduce the observed fields reasonably well although the results are still not really satisfactory (Youngblut and Sasamori, 1980).

It is, however, not only the time mean fields which exhibit strong zonal variations. If we look at the variability of the atmosphere at frequencies $|\omega| > 0$, we find pronounced variations along latitude circles. Sawyer (1970) and, more recently, Blackmon (1976) studied the variability of the 500 mb height for various frequency bands. They found, for example, that the 500 mb variability is dominated by low-frequency components ($2\pi/|\omega| = T > 10$ days) and that there are distinct maxima over the oceans, whereas the variability is reduced over the Rocky Mountains. At medium frequencies ($2.5 < T < 6$ days) maximum variability is found at the east coast of North America and over the central northern Pacific.

Only a few attempts have been made to explain these findings theoretically. For example, Frederiksen (1979) studied the instability of three dimensional baroclinic fields typical of the northern hemisphere average circulation and found maximum wave growth downstream of the jet stream maxima in the Pacific Ocean and off the coast of North America. It appears, therefore, that part of the variation of atmospheric variability with longitude with time scales of a few days may be due to variations of baroclinic activity.

Egger and Schilling (1983) studied the non-linear forcing of planetary modes by synoptic-scale systems over a wide range of frequencies and found that much of the low-frequency variability at 500 mb may be seen as a response of the planetary modes to the geographically varying forcing by smaller-scale systems. There are, however, other mechanisms which may contribute to the variability of the atmosphere. For example, the heating over land and sea varies in time as well as with locality. Therefore, thermal forcing will induce locally varying atmospheric response over a wide range of frequencies. Orographic forcing is another mechanism which contributes to the atmospheric variability. The wind impinging on the mountains varies in time. Therefore, we have time-dependent sources and sinks of vorticity in mountainous areas and we expect a frequency-dependent atmospheric response which depends on locality. We are concerned with this latter mechanism in this paper.

We stress that this kind of orographic forcing is essentially stochastic. The zonal wind hitting the mountains varies rather erratically and it would be unreasonable to specify this forcing as a function of time. Instead we have to prescribe the statistical characteristics of the forcing. Correspondingly, we shall not try to derive the atmospheric response as a function of time but we shall aim at deriving just the statistics of the response. This approach is not novel. For example, it has been used by Mak (1969), who studied the impact of stochastic midlatitude flow on the tropics. Hasselmann (1976) stressed its relevance for the climate problem. We are, however, not aware that this technique has been applied to orographically forced motions.

The method to be used will be outlined in Section 2. The simplest case, where the orography is restricted to one Fourier mode, will be considered in Section 3. In Section 4 the stochastic forcing is discussed for the circular mountain. Finally an attempt is made to apply the method to the orography of the northern hemisphere.

2. Stochastic orographic forcing

Our problem can be viewed as an extension of the work by Charney and Eliassen (1949). Charney and Eliassen studied the steady-state response to orographic forcing by the mean wind, while we study the atmospheric response to a randomly varying wind. We also use essentially the same tools as Charney and Eliassen: we assume that the linearized barotropic vorticity equation with β-plane geometry is capable of reproducing the essential features of large-scale flow outside the tropics. This equation reads

$$\frac{\partial}{\partial t}(\nabla^2 - \lambda^2)\,\psi + U_0 \frac{\partial}{\partial x}\nabla^2 \psi + \beta \frac{\partial \psi}{\partial x} = -C\nabla^2 \psi - \frac{u_s f_0}{H}\frac{\partial h}{\partial x}, \tag{2.1}$$

where $\psi(x, y, t)$ is the perturbation stream function, $h(x, y)$ is the orography, H a scale height and β, f_0 are middle latitude values of $\beta = \mathrm{d}f/\mathrm{d}y$ and of the Coriolis parameter, respectively. The perturbations ψ are deviations from a zonal mean state with zonal velocity U_0 which depends neither on time nor on y. The first term on the right-hand side is thought to provide a crude representation of frictional effects where C is a damping constant. Reasonable values of C are of the order 1–2×10^{-6} s^{-1}. The constant λ^{-1} is the radius of deformation. The second term on the right-hand side represents the orographic forcing of the perturbations, where u_s is the zonally averaged surface wind. We may write

$$u_s(y, t) = \bar{u}_s(y) + u_s'(y, t), \tag{2.2}$$

where $\bar{\mu}_s(y)$ is the time mean surface wind and u_s' the deviation. The response to the mean orographic forcing term $\sim \bar{u}_s\, \partial h/\partial x$ has been studied extensively in the past (see the references cited in Section 1). Since (2.1) is linear, the impact of forcing terms may be studied individually. Accordingly we can omit the mean orographic forcing and just retain the time-dependent part of the orographic forcing, thus replacing the second term of (2.1) by $-f_0 u_s'(\partial h/\partial x)/H$. The statistical characteristics of the surface wind deviations u_s' will be prescribed. We wish to emphasize that this approach contains a slight inconsistency. If the zonal flow impinges on mountains, momentum can be transferred and the zonal flow will change accordingly. Therefore the zonal flow U_0 on the left-hand side of (2.1) should depend on time. It will be shown, however, (Table 1), that these changes are so small, that the error made by assuming a constant U_0 is certainly tolerable within the framework of a linear theory. Note that we have also neglected latitudinal variations of the time mean zonal flow. These should be taken into account in a more advanced stage of the analysis.

We adopt a channel with periodic boundaries in the x-direction and solid walls as northern and

Table 1. *Statistical characteristics of the power spectra of the zonal wind fluctuations u_{sn} for $0 \leqslant n \leqslant 2$, after Schilling (personal communication)*

n	0	1	2
$R_n(0)$ ($m^2 s^{-2}$)	0.1	4.5	6.1
$\gamma_n(d^{-1})$	0.25	0.27	0.22

southern boundaries as the flow domain. We represent the stream function ψ in terms of the eigenmodes of the laplacian for this domain

$$\psi = \tfrac{1}{2} \sum_{m=1}^{M} \sum_{n=1}^{N} (\psi_{mn}(t) \exp(ik_m x) + \psi^*_{mn}(t) \exp(-ik_m x)) \sin l_n y, \tag{2.3}$$

with Fourier expansion coefficients ψ_{mn} where $k_m = 2\pi m/L$, $l_n = n\pi/B$. We denote the channel length by L, and its width by B. The basic modes have been chosen so as to have $\psi = 0$ at $y = B, 0$. The orography is expanded with expansion coefficients h_{mn}. The surface wind must be expanded as well

$$u'_s = \sum_{n=0}^{N} u_{sn} \cos l_n y. \tag{2.4}$$

Of course, $u'_s \sim \cos l_n y$ since $u = -\partial\psi/\partial y$. In particular, u'_{s0} is the area average of the time-dependent part of the surface wind. Inserting (2.3), (2.4) in (2.1) we obtain the prognostic equation for the expansion coefficients ψ_{mn}:

$$\frac{d\psi_{mn}}{dt} + i\omega_{Rmn}\psi_{mn} = \frac{iA_{mn}}{2}\left\{\sum_{r=0}^{n} u'_{sr}(h_{mn-r} + h_{mn+r}) + \sum_{r=n+1}^{N} u'_{sr}(h_{mr+n} - h_{mr-n})\right\} - \tilde{C}\psi_{mn}, \tag{2.5}$$

where

$$k^2_{mn} = k^2_m + l^2_n,$$
$$A_{mn} = k_m f_0/H(k^2_{mn} + \lambda^2),$$
$$\tilde{C} = C/(1 + \lambda^2/k^2_{mn}), \tag{2.6}$$

and where we have adopted the convention $h_{mn+r} = 0$ if $n + r > N$. The Rossby frequency of a mode (m, n) is

$$\omega_{Rmn} = (U_0 - \beta/k^2_{mn})k_m/(1 + \lambda^2/k^2_{mn}). \tag{2.7}$$

Next a Fourier transform in time is performed with

$$P_{mn}(\omega) = \int_{-\infty}^{+\infty} \psi_{mn}\, e^{i\omega t}\, dt. \tag{2.8}$$

Strickly speaking, a Fourier transform need not be bounded in a dissipative flow system. It is, however, easy to prove that the more appropriate Laplace transform would yield virtually the same results. Let $P(x, y, \omega)$, $q_{sr}(\omega)$ denote the transform of $\psi(x, y, t)$, $u'_{sr}(t)$, respectively.

Then the transform of (2.5) is

$$P_{mn} = \frac{A_{mn}}{2(\omega_{Rmn} - \omega - i\tilde{C})}\left(\sum_{r=0}^{n} q_{sr}(h_{mn-r} + h_{mn+r}) + \sum_{r=n+1}^{N} q_{sr}(h_{mr+n} - h_{mr-n})\right). \tag{2.9}$$

Switching back to physical space, we obtain the transform of (2.3)

$$P(x, y, \omega) = \tfrac{1}{2} \sum_{m=1}^{M} \sum_{n=1}^{N} (P_{mn}(\omega)\, e^{ik_m x} + P^*_{mn}(-\omega)\, e^{-ik_m x}) \sin l_n y. \tag{2.10}$$

We might proceed by transforming (2.10) back to the time domain. This would yield a succession of "weather maps" $\psi(x, y, t)$ which describe the response of the barotropic flow to an orographic forcing which changes in time. However, as discussed in Section 1, we are not interested in such a "deterministic" solution. We just want to derive the statistical characteristics of the response. Although there is quite a variety of statistical information one might want to extract from the equations, we shall restrict our attention to the computation of power spectra. The power spectrum of the stream function at a certain locality can be determined from (2.10), if we know the power spectra of u'_{sn}. We now turn to observations in order to find out about these spectra. Schilling (personal communication) took 2 years of daily height observations for the domain 15° N–85° N. Using geostrophic balance, he computed the zonal wind at 1000 mb from longitudinally-averaged height fields on an equidistant latitudinal grid. We shall use this estimated wind as surface wind. Then the autocovariance

$$R_n(\tau) = [u'_{sn}(t)\, u'_{sn}(t + \tau)] \tag{2.11}$$

was obtained, where the brackets stand for a time average over 2 years. The power spectrum is

$$S_n(\omega) = 2\int_0^{\infty} R_n(\tau) \cos \omega\tau\, d\tau. \tag{2.12}$$

Although we could use the power spectrum as derived from the data, it is more convenient to replace the observed power spectrum by a fitted spectrum. Schilling fitted the stationary Markov process of first order

$$u_{s\,n\,j+1} = u_{s\,n\,j} \exp(-\gamma_n) + ((1 - \exp(-2\gamma_n) R_n(0))^{1/2} W_j \tag{2.13}$$

to each time series of the coefficients u_{sn}, where j is a running index in time increasing by one every day. The symbol W_j stands for a white noise process with power one and γ_n is the parameter to be fitted. Table 1 shows the resulting values of γ_n and $R_n(0)$ for the first three modes of the 1000 mb zonal flow. The variance of u_{s0} is rather low. Therefore, the variations in time of the superrotational mode u_{s0} will hardly excite any significant response. The variances of both the other modes are much stronger. The decay parameters γ_n are quite small. This means that the first three modes of u_s have a high persistency. Fig. 1 shows the power spectrum of the surface wind component u_{s0}. Obviously the spectrum of u_{s0} is rather "red", i.e. most of the variance is concentrated at low frequencies. The spectra for the higher modes of u_s are quite similar to that shown in Fig. 1. Since only 2 years of data were available, it is the low-frequency part of the spectrum which is not well covered by the analysis. Therefore, the parameters listed in Table 1 must be seen as estimates with the correct order of magnitude.

We find from (2.13) an approximate formula for the autocovariance

$$R_n(\tau) = R_n(0) \exp(-\gamma_n \tau) \tag{2.14}$$

and the power spectrum

$$S_n(\omega) = R_n(0)\, \gamma_n/(\gamma_n^2 + \omega^2). \tag{2.15}$$

Fig. 1 shows the power spectrum $S_0(\omega)$ according to (2.15). There is good agreement of the observed and the computed spectrum, although the fitted spectrum overestimates the variability of u_{s0} for high frequencies.

Given the power spectrum of the zonal wind, we can compute the power spectrum $S(x, y, \omega)$ of the response. The computation is performed according

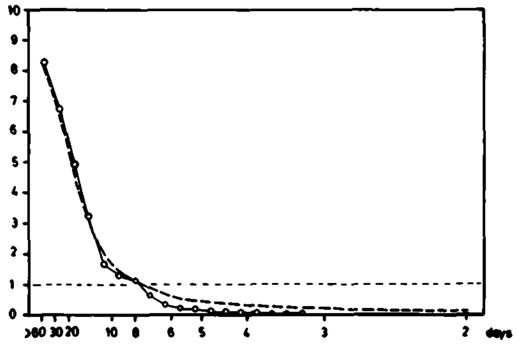

Fig. 1. Power spectrum of u_{s0} and the corresponding fitted power (dashed). The power is normalized with respect to a white spectrum for the same frequency interval.

to the following rule. We multiply $P(x, y, \omega)$ with its complex conjugate P^*. In doing so we have products of the form $q_{sp} q_{sg}^*$. These are to be replaced by the power spectrum $S_p(\omega)$ if $p = q$. The resulting formula will be given in Section 3 for the case of a single mode. If $p \neq g$ we neglect the corresponding term thus assuming that there is no correlation between different modes. Given all the approximations made so far, it would have been unreasonable to include such subtle effects as the correlations between zonal flow modes. The resulting expression is the power spectrum $S(x, y, \omega)$ of the response.

3. Power spectra for single modes

To resolve the large-scale flow of the northern hemisphere even coarsely, we need some 50–100 modes. Correspondingly, (2.10) is a rather lengthy and involved expression. It is therefore helpful to consider first the simplest case where we have only one mode (m, n) of the flow and where only u_{s0} is fluctuating. We are free to choose the position of the mountain

$$h = h_0 \sin k_m x \sin l_n y, \tag{3.1}$$

and have, therefore, $h_{mn} = -ih_0$. The mountain's crest is located at $x = L/4m$. We obtain from (2.9) after simple manipulations

$$P(x, y, \omega) = \frac{A_{mn}\, h_0\, q_{s0}(\omega_{Rmn} \sin k_m x + (\tilde{C} - i\omega) \cos k_m x) \sin l_n y}{(\omega_{Rmn}^2 - (\omega + i\tilde{C})^2)}. \tag{3.2}$$

Following the rule outlined in Section 2, we obtain the power spectrum

$$S(x, y, \omega) = \frac{A_{mn}^2 h_0^2 S_0(\omega) [(\omega_{Rmn} \sin k_m x + \tilde{C} \cos k_m x)^2 + \omega^2 \cos^2 k_m x] \sin^2 l_n y}{((\omega_{Rmn}^2 - \omega^2 + \tilde{C}^2)^2 + 4\tilde{C}^2 \omega^2)}. \tag{3.3}$$

To simplify matters further on, let us assume that the power spectrum of u_{s_0} is white: $S_0 = R_0/\gamma_0$. Since the dependence of S on y is trivial for the one mode case, we may omit the factor $\sin^2 l_{ny}$ in (3.3).

Since A_{mn} decreases with increasing wave number, we can conclude that only the large scales in the channel will contribute to the power. As can be seen from (3.3), S has a zonally averaged part $\bar{S}^*$ and a zonally varying part $\hat{S}$ with the wave number $2k_m$. We find

$$\bar{S}^* = A_{mn}^2 h_0^2 S_o(\omega_{Rmn}^2 + \omega^2 + \tilde{C}^2)/2((\omega_{Rmn}^2 - \omega^2 + \tilde{C}^2)^2 + 4\tilde{C}^2 \omega^2), \tag{3.4}$$

$$\hat{S} = \frac{A_{mn}^2 h_0^2 S_0((\tilde{C}^2 + \omega^2 - \omega_{Rmn}^2) \cos 2k_m x + 2\omega_{Rmn} \tilde{C} \sin 2k_m x)}{2((\omega_{Rmn}^2 - \omega^2 + \tilde{C}^2)^2 + 4\tilde{C}^2 \omega^2)} \tag{3.5}$$

The power S has two maxima and two minima in the interval $0 \leqslant x \leqslant L/m$. Let x_{max} denote the position of the maximum closest to the crest.

Fig. 2a shows the extremum $S_{max}(\omega) = S(x_{max}, \omega)$ of the power as a function of ω for a rapidly westward moving mode ($m = n = 1$; $T_R = 2\pi/\omega_R = -3.3d$) and a slow mode ($m = 5$, $n = 1$; $T_R = -36d$). The arrows in Fig. 2a mark the period $|T_R|$ for each mode. Maximum power $S_{max}(\omega)$ is obtained for a frequency ω_{max} which is close to ω_{Rmn}. This is not surprising since ω_{Rmn} is the mode's eigenfrequency for the frictionless case. The response to forcing with frequency ω should be largest close to ω_{Rmn} even if damping is included. Although ω_{max} can be determined exactly from (3.3), we assume here that S_{max} must be close to its largest value when the denominator of (3.3) is smallest. The denominator of (3.3) has an extremum if

$$\omega^2(\omega^2 - \omega_{Rmn}^2 + \tilde{C}^2) = 0. \tag{3.6}$$

The extremum is a minimum for

$$\omega_{max} = 0, \tag{3.7}$$

if $\tilde{C} > |\omega_{Rmn}|$ and for

$$\omega_{max} = \pm(\omega_{Rmn}^2 - \tilde{C}^2)^{1/2} \tag{3.8}$$

otherwise.

Fig. 2a shows that S_{max} (ω_{max}) depends on the mode chosen. The fast mode has more power than the slow mode. A close analysis reveals that this is due to the factor A_{mn}^2 in (3.3) which is larger for the mode (1, 1). However, if there are two modes with about equally large factors A_{mn}^2, the mode with the smaller Rossby frequency will have the larger power $S_{max}(\omega_{max})$. This is the more so if we use the more realistic "red" spectra of the zonal wind (2.15) which favour the power at low frequencies.

Fig. 2a also shows the minimum S_{min} of the power in the interval $0 \leqslant x \leqslant L/2m$. It is seen that the minimum comes close to S_{max} for the mode (5, 1). According to (3.4), (3.5), the quotient Q of the amplitude of $\hat{S}$ and $\bar{S}$ is

$$Q(\omega) = \{(\tilde{C}^2 + \omega^2)^2 + \omega_{Rmn}^4 + 2\omega_{Rmn}^2 \tilde{C}^2 - 2\omega^2 \omega_{Rmn}^2\}^{1/2}/(\omega_{Rmn}^2 + \omega^2 + \tilde{C}^2). \tag{3.9}$$

Now if $\omega_{max}^2 \gg \tilde{C}^2$, we have $Q(\omega_{max}) \sim 0$. Therefore fast modes like (1, 1) do not create a lot of variation of the power with x. The response has about the same intensity everywhere in the channel, at least for the frequencies close to ω_R. On the other hand if $\omega_R^2 \sim \tilde{C}^2$ we find by aid of (3.8)

$$Q \simeq \tilde{C}/|\omega_{Rmn}| \simeq 1. \tag{3.10}$$

This means that we have to expect rather pronounced variations of the power with x for modes like (5, 1) where $\tilde{C} \sim |\omega_R|$, and that is what we see in Fig. 2a.

Let us briefly comment on the sensitivity of the response to the choice of the radius of deformation λ^{-1}. In Fig. 2a, we had $\lambda = 0$. Fig. 2b shows $S_{max}(x_{max}, \omega)$ for the same modes but for $\lambda = 1 \times 10^{-6}$ m^{-1}, a value thought to be typical of large-scale flow (Wiin-Nielsen, 1959). Obviously, the mode (5, 1) is not strongly affected by this choice. However, the mode (1, 1) now has a rather sharp peak at low frequencies. The reason for this change is obvious. According to (2.7), ω_{Rmn} is rather sensitive to changes of λ^2 for small wave numbers.

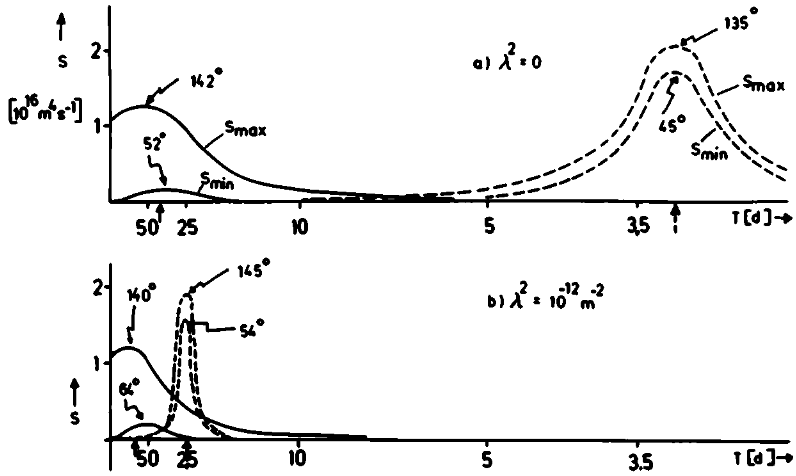

Fig. 2. S_{max} and S_{min} as functions of the period $T = 2\pi/\omega$ for the modes (1, 1) (dashed) and (5, 1) full. The arrows mark the Rossby period of the modes. Phase angles of the positions of the extrema $S_{max}(\omega_{max})$, $S_{min}(\omega_{max})$ in degrees. $U_0 = 10$ m s^{-1}; $C = 2 \times 10^{-6}$ s^{-1}; $h_0 = 100$ m; $L = 28 \times 10^6$ m; B = 10×10^6 m. See text for further explanation.

4. Spectra for a circular mountain

If we turn to the flow over realistic topography in a channel, we have to include many modes to properly represent the flow. Then the power spectra of the stream function are truly two-dimensional and can be understood only by studying the superposition of many wave modes. Nevertheless, we may be able to explain at least part of the results by recalling the main results of the foregoing analysis.

(i) A mode in the channel contributes maximally to the power near the Rossby frequency ω_{Rmn} of that mode.

(ii) This contribution tends to decrease with increasing wave number.

(iii) The slow modes with $|\omega_{Rmn}| \leqslant \tilde{C}$ are most effective in producing zonal variations of the power S.

Let us first look at a situation which has been treated quite often within the framework of linear steady-state theory. We have a circular mountain of 500 m height and a diameter of about 2000 km embedded in westerly flow. To simplify matters, we assume that we have fluctuations of u_{s0} only, and that the spectrum of u_{s0} is white.

Fig. 3 shows the power S (x, y, ω) at the frequency $\omega = 2\pi/T$, $T = 20$ d, for a mean flow $U_0 = 10$ m s^{-1} and for $\lambda^2 = 0$. We obtain a train of circular maxima downstream of the obstacle. The amplitude of the maxima decreases with distance to the mountain. There is also a weak maximum on the windward side of the mountain.

To understand Fig. 3, we may ask first for which modes the Rossby period T_R is about equal to 20 d. For example, the mode (4, 4) has a Rossby period of 24.6 d, the mode (3,5) has 23.8 d. The wave length $L_{mn} = 2\pi/k_{mn}$ of these modes comes rather close to the wave length $L_R = 2\pi(U_0/\beta)^{1/2} \sim 5 \times 10^6$ m of the free stationary Rossby waves. We see indeed that the circular crests of S in the lee of the mountains have a distance of $L_R/2$. Thus the variations of S along the channel's axis are largely in agreement with (iii).

The response in Fig. 3 is restricted to the lee. This feature must be due to the superposition of the many modes excited by the mountain, an effect not included in the analysis of Section 3. To understand Fig. 3 more fully, we have to invoke the theory of the propagation of wave packets on the β-plane (e.g. Lighthill, 1966). According to Lighthill an obstacle embedded in westerly flow on an infinite β-plane creates a steady-state downstream wave train with a circular wave pattern centred at the mountain. The wavelength of the pattern is L_R. Since the group velocity of the Rossby waves is positive, there is no response upstream. This pattern is modified by the walls of the channel but the modification is small if the mountain is located at the channel's axis (Egger, 1982). The power $S(x, y, \omega)$ displayed in Fig. 3 fits this description rather nicely. The frequency is so small that the

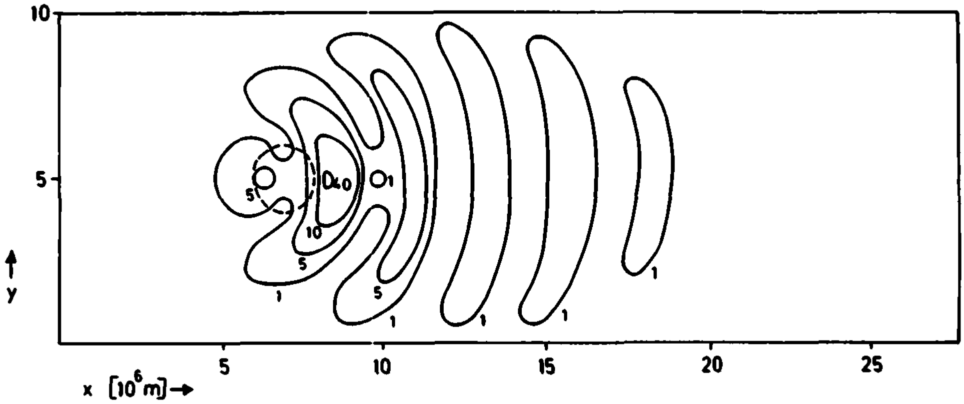

Fig. 3. Power S (10^{14} m^4 s^{-1}) at $T = 20$ d induced by randomly fluctuating mean flow u_{s0} impinging on a circular mountain of 500 m height. Circumference of mountain dashed. Numerical resolution $M = 20$, $N = 7$. $U_0 = 10$ m s^{-1}; $C = 2 \times 10^{-6}$ s^{-1}; $\lambda = 0$; white noise forcing $S_0 = 1$ m^2 s^{-2} d.

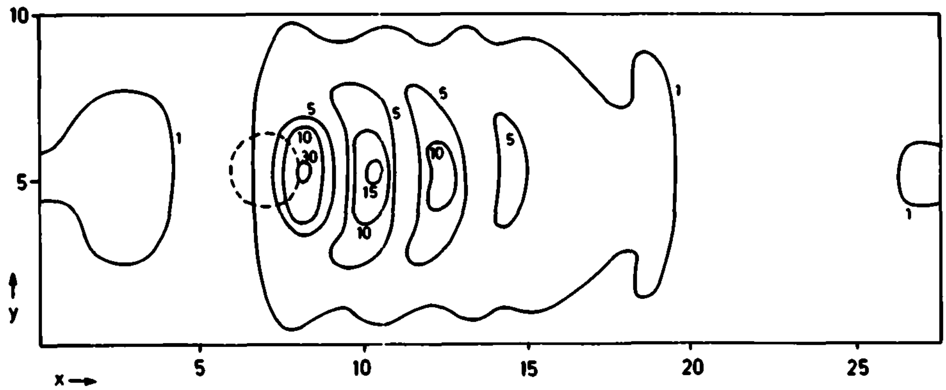

Fig. 4. The same as Fig. 3 but for $T = 4$ d.

response to the fluctuations of U_0 at this frequency should be close to the steady state response. Therefore, we have to expect maxima of S at the ridges and troughs of the steady state pattern and that is what we see in Fig. 3.

The response is similar to that displayed in Fig. 3 if we consider a barotropic medium with a free surface ($\lambda = 1 \times 10^{-6}$ m^{-1}). We still have a series of circular crests in the lee. However, the power of the first maximum in the lee is increased by about 20% and the power is larger now upstream of the mountain. In particular, we have a maximum of $\sim 1 \times 10^{14}$ m^4 s^{-1} at $x \sim 26 \times 10^6$ m. It is the mode (1, 1) which is responsible for this maximum. As has been discussed in the foregoing (Fig. 2), the mode (1, 1) is fast moving for $\lambda = 0$ but is almost resonant at $T = 20$ d ($T_R = 25$ d) for $\lambda = 1 \times 10^{-6}$.

If the period of the fluctuations μ_s' is decreased to 4 days (Fig. 4) we obtain patters of S which are similar to those seen in Fig. 3. There is no upstream response and an array of attenuating crests downstream. One can show that it is again the modes with $\omega \sim \omega_{Rmn}$ which dominate the response. However, the proof is more complicated now since there are two resonating wave numbers

$$k_{mn} = (-\omega \pm (\omega^2 + 4\beta U_0)^{1/2})/2U_0 \tag{4.1}$$

and we shall not enter a detailed discussion.

If we admit stochastic forcing by zonal wind components with $n \geqslant 1$, we have to take into account the interaction rules as given in (2.9). Let us again consider a circular mountain at the channel axis. In that case $h_{mn} = 0$ for n even. Now if we have stochastic forcing by u_{s1}, we see from (2.9) that only flow modes with even meridional wave numbers can be excited. In particular, $\psi = 0$ at the channel axis. If, on the other hand, u_{s2}' is chosen as stochastically varying zonal wind, we

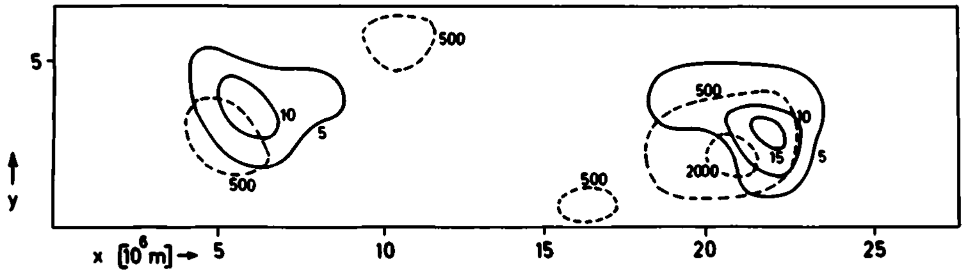

Fig. 5. Power S (10^{17} m^4 s^{-1}) at T = 20 d. Northern hemisphere orography height lines (m) dashed. Crosses mark the positions of additional maxima of S. $U_0 = 5$ m s^{-1}; $C = 2 \times 10^{-6}$ s^{-1}; $\lambda = 10^{-6}$ m^{-1}; red noise zonal wind fluctuations according to (2.15) and Table 1; $M = 9$, $N = 6$.

find that only flow modes with odd wave numbers can be excited just as was the case for u_{s0}. In fact, the response to forcing by u'_{s2} is fairly similar to that shown in Fig. 3.

5. Northern hemisphere orography

Once we turn to the complicated orography of the northern hemisphere, we can no longer expect to find such relatively simple lee wave patterns as for the circular mountain. Nevertheless, the wave dynamics are the same and, therefore, we ought to find power fields with similar characteristics. First we have to choose a flow domain. After all there is no immediately obvious correspondence between the hemisphere and a β-plane channel. Therefore, some arbitrariness is inevitable. We choose a channel with its axis at 45° N and length L = 28,000 km, the mid-latitude circumference of the earth. The channel width is 60° so that the southern wall is at 15° N and northern wall at 75° N. This choice is motivated by the fact that β-plane geometry distorts the spherical geometry most strongly near the pole. Furthermore, the tropical easterlies act as a barrier for wave propagation. Therefore, a wall at 15° N is not altogether unrealistic. However, we have to be aware that any such choice is rather problematic. As we have seen in the foregoing, resonant modes are important in determining the power of the response. These modes are typical of the channel chosen and therefore, the response depends to some degree on the geometry of the channel. Any comparison with observed power fields must be highly doubtful under such circumstances. On the other hand, the response close to a mountain is relatively independent of the channel geometry.

Thus, we can only obtain an order of magnitude estimate of the scale and intensity of the power of the fluctuations induced in the atmosphere by the interaction of the stochastically-varying zonal flow with the orography. Also, the modes of u'_s chosen by Schilling are somewhat different from those used here.

The orography of the northern hemisphere is read off a (λ, ϕ) grid, but damped to zero near the walls of the channel. This procedure is necessary since the orographic profile is to be expanded in a Fourier series with $h = 0$ at the walls. We use a resolution of 9 zonal wave numbers and 6 meridional wave numbers.

Fig. 5 shows the orography in the channel as well as the power of the stream function for a period of 20 d. We have chosen a zonal wind forcing with 3 modes given in Table 1. The interpretation of Fig. 5 is not difficult. Both the Himalayas and the Rocky Mountains set up a lee wave pattern in analogy to Fig. 3 with a pronounced maximum of power in the lee and a weaker maximum on the windward side. There are no distinct secondary maxima downstream. This may be due to interference of the wave systems created by the Himalayas and the Rocky Mountains. What is left of Greenland in our channel appears to be too small and too close to the wall to induce a significant downstream response. We have also computed the variance of the response for the low-frequency fluctuations with periods between 10 and 100 d. This variance is obtained by integrating the power over the corresponding frequency band. Fig. 6 shows the corresponding standard deviation of the 500 mb height, where we have converted stream functions into geopotential height values by use of the geostrophic relation: $\psi f_0 = \phi$. According to our computations, the stochastic mountain forcing induces low-frequency height fluctuations

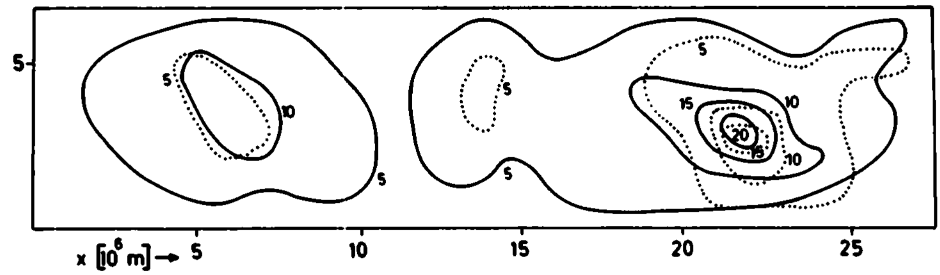

Fig. 6. Standard deviation (m) of the 500 mb height field as induced by randomly fluctuating zonal winds for periods $10 \leqslant T \leqslant 100$ d. Northern hemisphere orography; $U_0 = 5.0$ m s^{-1}; $C = 2 \times 10^{-6}$ s^{-1}; $\lambda = 10^{-4}$ m^{-1}; response for $\lambda = 0$ dotted; $M = 9$, $N = 6$.

with mean amplitudes of more than 20 m east of the Himalayas. Another maximum is found near the Rocky Mountains with about 10 m amplitude. We may compare the computed response to the observed low-frequency standard deviations of the 500 mb height field of Blackmon (1976). He found centres of long-term variability over the oceans with maximum values of 160 m and a mid-latitude zonal mean of order 100 m. If we accept Fig. 6 as an estimate of the orographically induced variability, we have to conclude that the interaction of the zonal wind and the orography is responsible for but a small fraction of the total low-frequency variability.

The only possible exception occurs to the east of the Himalayas where the strength of the orographically induced perturbations is large enough to potentially show up in the data. The charts of Blackmon (1976) show a minimum of the variability at 100–110° E, 30° N with a sudden increase along the coast of Asia near 120° E. Therefore, there is a minimum of the power slightly to the east of the Himalayas and an increase 20–30° east of the Himalayas. This does not really agree with our findings, and we conclude that we are not able to identify any one of the features seen in Fig. 6 in maps of the observed long-term variability.

A few more experiments have been carried out in order to check the sensitivity of the results to the parameters of our model. For example, reducing the damping factor to 1×10^{-6} s^{-1} resulted in an increase of the variance level by almost a factor of two, but the maximum in the Himalayan lee increased to just 26 m. The results are not sensitive to a change in the mean wind U_0. We obtain almost the same fields as displayed in Fig. 6 if we choose $U_0 = 10$ m s^{-1} or $U_0 = 15$ m s^{-1}.

Fig. 6 also shows the response to stochastic forcing for an atmosphere with a rigid lid (dotted). It is seen that putting $\lambda = 0$ results in a weakening of the response, but the overall variance pattern is nearly the same as for the free surface case.

6. Conclusion

We have studied the perturbations of a barotropic atmosphere induced by stochastically varying zonal flows impinging on mountains. Following Schilling (personal communication), we assumed red power spectra for the zonal flow fluctuations as a fit to observed spectra. The response to this stochastic mountain forcing has been evaluated for β-plane channel flow governed by the linearized barotropic vorticity equation.

First a one-mode case with a sinusoidal mountain has been analysed. In this case, the power spectra of the response can be discussed by simple analytic means. The mountain induces perturbations, the power of which depends on locality and, of course, on frequency. As one would have expected, the response is strongest for frequencies which are close to the Rossby frequency ω_R of that mode, i.e. the response spectra generally are not red. The variations of the power in space are most pronounced for slow modes with $\omega_R \sim \bar{C}$.

Next, the effect of a stochastically varying zonal flow interacting with a circular mountain was examined. The most pronounced maxima of the power are found in the lee and it has been shown that most features of the resulting power fields can be understood on the basis of the theory of Rossby wave packet propagation on an infinite β-plane. Most of the variance of the induced fluctuations is contained in the low-frequency part of the spectrum.

Finally an attempt has been made to determine the response for the orography of the northern hemisphere at mid-latitudes. Since the forcing has a realistic spectrum, we ought to be able to estimate the contribution of the stochastic orographic forcing to the variability of the atmosphere. It has been found that it is only in the lee of the Himalayas that the orographically forced low-frequency variability is comparable in magnitude to the observed variability of the atmosphere. However, the observed long-term variability has a minimum in the lee of the Himalayas. This suggests that stochastic orographic forcing is nowhere a main contributor to the atmospheric low-frequency variability. However, limitations of our model make it difficult to draw definite conclusions. For example, a model based on spherical geometry would have yielded different results (e.g. Hoskins et al., 1977). In particular wave trains excited by obstacles propagate differently on the sphere as compared to the β-plane. However, there is no evidence that the response close to the mountains would differ. Since that is where the response is strongest, the β-plane solutions appear to be acceptable. It is more difficult to find out how realistic our forcing is. After all, we allow only for stochastic variations of the zonally-averaged wind. It is quite likely, however, that large-scale weather systems passing over mountain chains excite responses which are at least as strong as those created by the variations of the zonal wind. These interactions would be described by a term $J(\psi, f_0\ \psi/H)$ in the vorticity equation and one could try to prescribe this term as a stochastic forcing term as well. The resulting response might be rather different from that presented in Fig. 6, but we would still expect to find a maximum response in the lee of the Himalayas. It is therefore a nagging question why we observe a minimum of the variance in the lee of the Himalayas and not a maximum. This could be a data problem since data coverage is not good in this area. Therefore it is difficult to obtain reliable estimates of the low-frequency variability there. On the other hand, long-term integrations carried out with a GCM also show a minimum of variability in the lee of the Himalayas (Manabe and Hahn, 1982). This suggests that our basic formulation of the problem as given by (2.1) is not very realistic when applied to the Himalayas. After all, the Himalayas are not small obstacles with $h \ll H$, nor are they embedded in strictly westerly flow. Instead the height of the Himalayas is of the same order of magnitude as the scale height of the atmosphere, and the Himalayas set up a circulation of their own which is not included in our treatment of the problem. Thus it would appear premature to draw any final conclusions with respect to the importance of stochastic orographic forcing. In particular, incorporation of three-dimensional effects might alter our conclusions profoundly.

7. Acknowledgement

The author is grateful to H. D. Schilling for making available his unpublished results on the stochastic characteristics of the zonal flow and to R. Hoffman and an anonymous referee for their constructive criticism.

REFERENCES

Blackmon, M. 1976. A climatological spectral study of the 500 mb geopotential height of the northern-hemisphere. *J. Atmos. Sci. 33*, 1607–1623.

Charney, J. and Eliassen, A. 1949. A numerical method for predicting the perturbations of the middle latitude westerlies. *Tellus 1*, 38–54.

Egger, J. 1982. Wave propagation in β-plane flows. *Contrib. Phys. Atmos. 55*, 170–176.

Egger, J. and Schilling, H.-D. 1983. On the theory of the long-term variability of the atmosphere. *J. Atmos. Sci., 40*, 1073–1085.

Frederiksen, J. S. 1979. The effect of long planetary waves on the regions of cyclogenesis: linear theory. *J. Atmos. Sci. 36*, 195–204.

Hasselmann, K. 1976. Stochastic climate models, Part 1, Theory. *Tellus 28*, 473–486.

Hoskins, B. J., Simmons, A. J. and Andrews, D. G. 1977. Energy dispersion in a barotropic atmosphere. *Q. J. R. Meteorol. Soc. 103*, 553–667.

Lighthill, M. J. 1966. Dynamics of rotating fluids: a survey. *J. Fluid Mech. 26*, 411–431.

Mak, M.-K. 1969. Laterally driven stochastic motions in the tropics. *J. Atmos. Sci. 26*, 41–64.

Manabe, S. and Hahn, D. 1981. Simulation of atmospheric variability. *Mon. Wea. Rev. 109*, 2260–2286.

Sawyer, J. S. 1970. Observational characteristics of atmospheric fluctuations with a time scale of a month. *Q. J. R. Meteorol. Soc. 96*, 610–625.

Wiin-Nielsen, A. 1959. On barotropic and baroclinic models, with special emphasis on ultralong waves. *Mon. Wea. Rev. 87*, 171–183.

Youngblut, C. and Sasamori, T. 1980. The non-linear effects of transient and stationary eddies on the winter mean circulation. Part I: Diagnostic analysis. *J. Atmos. Sci. 37*, 1944–1957.